# Grand Canonical Simulations of Hard-Disk Systems by Simulated Tempering

Gunter Döge[(1)], Klaus Mecke[(2)], Jesper Møller[(3)], Dietrich Stoyan[(1)] , and Rasmus P. Waagepetersen[(3)]

[(1)] *Institut für Stochastik, TU Bergakademie Freiberg, D-09596 Freiberg, Germany*

[(2)] *Fachbereich Physik, Bergische Universität Wuppertal, D-42097 Wuppertal, Germany*

[(3)] *Department of Mathematical Sciences, Aalborg University, DK-9220 Aalborg Ø, Denmark.*

(March 21, 2000)

www.maphysto.dk

MPS-RR 2000-11

ISSN 1398-599X

## Abstract

We present the application of simulated tempering for grand canonical hard-disk systems as an efficient alternative to the commonly used Monte Carlo algorithms. This approach allows the direct study of the packing fraction as a function of the chemical potential even in the vicinity of the melting transition. Furthermore, estimates of several spatial characteristics including pair correlation function, hexagonality number, and alignment function are studied in order to test the accuracy of the method and to analyze the melting transition in hard-disk systems. We find evidence for a weak first order phase transition.

## I. INTRODUCTION

The nature of the two-dimensional melting transition has been a matter of hot debate for the past three decades. Whereas a conventional first-order transition between the isotropic liquid and the solid was assumed since the pioneering work in 1962 by Alder

and Wainwright[1], the scenario of dissociation of dislocations and disclinations in the solid phase was proposed 1979 by Nelson, Halperin and Young[2], which leads to two second order transitions according to the theory by Kosterlitz and Thouless[3]. The intermediate so-called 'hexatic' phase displays an exponential decay of translational order, but an algebraic decay of bond orientational order. This is in contrast to the two-dimensional solid phase, where the bond orientational order is long ranged and the translational order decays algebraically. Even for a very simple system like hard disks, the issue of the order of the melting transition is not yet settled. For instance, hysteresis loops occurring at first order transitions depend strongly on system size in any simulation at fixed particle numbers. Therefore, large scale computer simulations or novel algorithms are needed which circumvent the ambiguities of the results obtained by conventional techniques.

Simulation algorithms such as the usual Metropolis algorithm[4] and molecular dynamics[5,6] play an important role in statistical physics (see[7–9]). These methods are also important tools in the study of canonical Gibbs hard-disk and hard-sphere systems with a fixed number of objects in a bounded set. Recent Monte Carlo simulations were done in the $NVT$ ensemble (constant volume)[10–12] and in the $NPT$ ensemble (constant pressure)[13,14], but none in the grand-canonical $\mu VT$ ensemble (constant chemical potential) because of the obvious difficulty to add a hard-core particle at high densities. Although numerical investigations of the two-dimensional melting could be done in several ways, the $NVT$ and $NPT$ simulations do not give conclusive results neither on the location of the melting ($\eta_s$) and freezing ($\eta_f$) densities, i.e., on the highest (lowest) possible density at which the pure fluid (solid) phase exist, nor on the nature of the transition itself.

The classical simulation work on hard-disk freezing transition by Alder and Wainwright found a first order transition[1,15], what is supported by more recent computer simulations[13,16]. But the data in Ref.[13] are limited to small particle numbers of about 400. Increasing the number up to 16384 still indicates a first order transition[10], but cannot rule out a continuous fluid-solid phase transition in the thermodynamic limit, i.e., a vanishing density discontinuity found in another simulation[14]. A first-order phase transition is supported by the study of

bond-orientational order, which rules out the existence of a hexatic phase[11]. However, the hexatic phase is stable in a system interacting with an $r^{-12}$-potential[17]. Also in experiments of PMMA particles squeezed to two dimensions by confinement between plates, the hexatic phase was found to be thermodynamically stable[18]. The existence of such a hexatic phase in the hard-disk system was recently found in Monte Carlo simulations of systems up to 65536 particles[19].

Concluding one can say that simulations support basically two main scenarios for the hard-disk system: a first order freezing transition with a finite density jump, similar to the three-dimensional case, and, alternatively, the existence of a third phase with a hexatic structure between the fluid and the solid phase. The corresponding two phase transitions, fluid/hexatic and hexatic/solid, are proposed to be continuous according to the Kosterlitz-Thouless-Halperin-Nelson-Young scenario.

The aim of this paper is to point out that previous simulations performed at fixed particle number have several serious drawbacks and that grand canonical simulations may help to overcome these difficulties.

## II. DISCUSSION OF SIMULATION TECHNIQUES FOR TWO-DIMENSIONAL HARD-DISK SYSTEMS

Two-dimensional solids differ from three-dimensional ones in lacking long-range translational order, which arises from a divergence of long-wavelength fluctuations. Therefore, large system sizes are important for simulations of two-dimensional systems at fixed particle number in order to allow for significant fluctuation contributions to entropy. It is found in many simulations that for small particle number the system exhibits significantly more order than for larger numbers with the same density. In order to explore the properties of these less ordered states one has either to simulate very large ensembles or to allow fluctuations of particle number by sampling a grand canonical system. Otherwise the solid structure is stabilized what eventually may completely suppress a transition into a less ordered phase

until the solid structure becomes unstable close to the freezing density $\eta_f$. This results in a tie line between liquid ($\eta_f$) and solid ($\eta_s$) phase, which moves to smaller chemical potentials $\log z$ and becomes shorter than in an equilibrium simulation.

In particular at high densities, simulations with a fixed number of particles suppress in a systematic way configurational fluctuations. Similarly to the single-occupancy cell approximation, particles are almost surely constrained to motions within a single cell defined by their neighbours. This unrealistic restriction is due to the low acceptance rate of 'large moves' in conventional Monte Carlo simulations consisting of deleting and adding a particle at another position. Usually all particles are moved only maximally one tenth of the radius at each update in order to achieve an acceptable rate, which nevertheless makes the convergence very slow and suppresses large scale fluctuations. Thus in usual computer simulations with fixed particle number any particle almost never leaves its cell. This is obviously the case for fixed volume simulations ($NVT$ ensemble), but even in fixed pressure simulations ($NPT$ ensemble) only an overall scaling of distances, i.e. an isotropic change of volume, is performed which does not change the configuration or the respective arrangement of the particles. Thus we expect the solid phase to be stabilized by all simulation techniques so far applied, making the need of another method obvious.

It has been observed quite often in small hard-disk systems that after $10^6$ Monte Carlo sweeps highly ordered configurations evolve suddenly into less ordered ones. Although this equilibration time decreases with system size, the number of updates in a run which are needed for good statistics is generally larger than $10^7$ because of the long persistence of the apparently metastable solid. Even for simulations of that size one cannot be sure whether one has reached the thermodynamic limit or whether the disorder of an apparent solid structure would increase further if larger systems were studied for longer running times. But the tie line between the coexisting fluid and solid phases could become larger because of a phase transition at a higher pressure induced by disorder. If simulations can be performed on systems large enough to allow sufficient disorder to come in, the resulting increase in pressure shifts the melting density $\eta_s$ to larger values.

There seem to be two ways to circumvent this uncomfortable situation. The first one is to extend the system to very large size and time scales which allow long range fluctuations.

The second possibility, namely simulating a grand canonical ensemble with fluctuating particle number, is commonly rejected because of 'obvious reasons'. But we will show in Section III that simulated tempering makes such simulations possible even for hard disks at high densities so that grand canonical simulations are not hampered in the high-density regime anymore.

Even in large systems of macroscopic size many metastable states are encountered in simulations which can be annihilated only by sufficiently large fluctuations available in an 'infinite system'. But in systems of finite size, in particular in the small systems usually treated on computers, metastable phases persist for a long time. Most simulations at high densities start from perfect lattice configurations, which would melt below the melting transition. But nevertheless for densities in the transition regime, the crystal is assumed to be stabilized by the initial conditions. Due to the irregular spatial structure of a fluid, it is difficult to invent a simulation method which stabilizes a fluid in the transition regime. Such a technique would allow to determine $\eta_s$ more precisely than $\eta_f$ and would be a complementary approach to simulations at fixed particle number.

Since one can suspect that most simulations stabilize the solid phase at densities for which it would melt already, it seems to be necessary to implement a simulation technique which stabilizes the fluid phase (which allows for metastable fluid configurations) but decreases the stability of solid configurations. Perhaps, large system sizes are not necessary for such simulations since large scale fluctuations are introduced by particle exchange, i.e., deleting and adding hard discs.

There are two other important reasons for an implementation of grand canonical simulations, namely 1) the possibility of direct determination of the entropy in the solid phase and 2) to overcome the constraints on the lattice structure induced by periodic boundary conditions:

1) In the fluid phase both pressure and free energy (or entropy) are known since one

has a continuous path to the ideal gas limit, which can serve as a reference system with known thermodynamic quantities. But in the solid phase the entropy is also known by integration techniques, except for an additive constant which cannot be determined directly. This difficulty arises because the entropy, a part of the chemical potential, is not a function of coordinates (dynamical variable) which can be averaged but is defined relative to a reference system by integrating along a reversible path to the considered state. In simulations with a fixed number of particles one has no possibility to determine the entropy and to compare the amount of disorder by analytical results on the solid side of the transition. This is only possible for grand canonical simulations. Additionally, a grand canonical simulation would not only allow direct determination of entropy and the additional constant in the solid phase but also measurement of the van der Waals loop $\lambda(z)$ in the transition regime.

2) In order to minimize the influence of the simulation box upon the spatial structure of the solid phase, one can apply periodic boundary conditions on a rectangular box of aspect ratio $\sqrt{3} : 2$ allowing hexagonal lattice structures. Nevertheless, in canonical systems with fixed particle numbers such devices are by no means sufficient to avoid influences of the boundary conditions on the solid structure. For instance, the net number of vacancies, i.e., the difference of vacancies and interstitial particles is constant[20]. Since in most canonical simulations the net number of vacancies is set equal to zero, the configurations will probably never reach globally full equilibrium. The hope when applying large scale simulations is that local subsystems exhibit random boundaries and resemble a multicanonical system which is large enough to reach equilibrium values of thermodynamic quantities. One could avoid in principle such problems by applying grand canonical simulations.

The grand canonical case with a random number of objects cannot be attacked by molecular dynamics and is difficult with commonly used Metropolis-Hastings algorithms in the neighborhood of the melting and freezing point. In this situation and probably in many other cases a novel method called simulated tempering[21,22] may be helpful. It is able to improve greatly the mixing properties of Metropolis-Hastings algorithms.

The idea of simulated tempering applied to a system with a high degree of order is to carry

out simulations for a series of coupled systems which work under different 'temperatures'. The 'coldest' system is that system which has really to be simulated, where Metropolis has unsatisfactory mixing properties, while the 'hottest' is completely random. In the case of simulation of hard-disk systems, overlappings of disks in different extents in the stages above the cold system are possible. During the simulation, the process moves randomly up and down between the various systems, producing samples of the cold systems during stays in that system. The price of this procedure is a more sophisticated simulation approach and a bit more computer storage space. Perhaps, the simulated complex system with the various stages may have an own physical meaning.

The aim of the present paper is to explain the application of simulated tempering to simulation of grand canonical Gibbs hard-disk systems. In Section III we introduce and compare the algorithms. The results of simulated tempering simulations are reported in Section IV. It represents, for instance, the functional relationship between packing fraction $\eta$ and the fugacivity parameter $z$; $\log z = \mu$ is the chemical activity. For values of $z$ below the freezing point the Padé approximation for the fluid phase[23,24] and the simulation results are in very good agreement. Similarly, a cell model approximation and the simulation results for $z$ above the melting point are close together. Finally, the simulated tempering simulations produce similar pair correlation functions as those presented in Truskett *et al.*[25], which were obtained by molecular dynamics.

## III. GRAND CANONICAL SIMULATIONS FOR HARD-DISK SYSTEMS

We consider a planar hard-disk Gibbs process with disk diameter $d$ and chemical activity $\log z$. Denote by $\lambda(z)$ the corresponding intensity or density of disks, i.e., the mean number of disks per unit area. The intensity is connected with the packing fraction $\eta(z)$ by $\eta = \lambda\frac{\pi}{4}d^2$. Discontinuities of $\eta(z)$, if they exist, are associated with coexisting densities at a phase transition. Simulation results indicate the existence of a phase transition between the 'freezing point' $\eta_f = 0.69$ and the 'melting point' $\eta_s = 0.716$[25–27].

In order to investigate such properties one has to resort to computer simulations of a hard core Gibbs process defined on a bounded region $W$. A hard-disk configuration $\varphi$ is denoted by $\varphi = \{\vec{x}_1, \ldots, \vec{x}_{\#\varphi}\}$, where $\#\varphi$ is the number of disks with centres in $W$ and the $\vec{x}_i$'s are the centres of the disks. In grand canonical simulations that number $\#\varphi$ is variable. The corresponding probability density is

$$f(\varphi) = \frac{1}{\Xi} z^{\#\varphi} \exp\left( - \sum_{1 \le i < j \le \#\varphi} V\left(\|\vec{x}_i - \vec{x}_j\|\right) \right) \tag{3.1}$$

with the hard-core pair potential

$$V(r) = \infty \quad \text{if } r < d, \quad V(r) = 0 \quad \text{else.} \tag{3.2}$$

The normalization factor $\Xi$ is the well-known grand canonical partition function

$$\Xi = \sum_{N=0}^{\infty} \frac{z^N}{|W|^N N!} \int_{W^N} \exp\left( - \sum_{1 \le i < j \le N} V\left(\|\vec{x}_i - \vec{x}_j\|\right) \right) \mathrm{d}\vec{x}_1 \ldots \mathrm{d}\vec{x}_N. \tag{3.3}$$

In the simulations discussed here, $W = [0, a]^2$ is a square and the periodic boundary condition is used, here and henceforth,

$$\|\vec{x}\| = \left( \left(\min(x_1, a - x_1)\right)^2 + \left(\min(x_2, a - x_2)\right)^2 \right)^{1/2} \tag{3.4}$$

denotes the geodesic distance when $W$ is wrapped on a torus.

The simulation problem becomes difficult when $z$ increases. In order to obtain a simulation algorithm with good mixing properties, various Metropolis-Hastings algorithms are combined with simulated tempering.

The basic algorithm is the Metropolis-Hastings algorithm studied in Geyer and Møller[28], Geyer[29] and Møller[30]. The following provides a short description of the Metropolis-Hastings algorithm; note that it covers the canonical ensemble as well as the grand canonical ensemble. After this, the combination of the Metropolis-Hastings algorithm and simulated tempering[21,22] will be described.

## A. Basic Metropolis-Hastings Algorithm

It is convenient to describe the Metropolis-Hastings algorithm for the case of simulation from any Gibbs process density $f$ in (3.1), i.e., for arbitrary pair potential $V$. Metropolis-Hastings is a special variant of Markov Chain Monte Carlo, the general principle is to create a Markov chain $\{\Phi_l\}_{l=0,1,\ldots}$ whose equilibrium distribution is $f$ and then to simulate this Markov chain.

Assume that $\varphi$ with $f(\varphi) > 0$ is the current state of the Markov chain generated by the Metropolis-Hastings algorithm. It is then proposed to either (a) insert, (b) delete, or (c) move a disk with probabilities $p^{\mathrm{ins}}$, $p^{\mathrm{del}}$, and $1 - p^{\mathrm{ins}} - p^{\mathrm{del}}$, respectively. In general the probabilities $p^{\mathrm{ins}}$ and $p^{\mathrm{del}}$ can be chosen dependent on $\varphi$, but in our simulations they are constant. The proposal $\varphi'$ for the next state in the chain is taken as follows:

(a) $\varphi' = \varphi \cup \{\vec{x}\}$, where the new point $\vec{x} \in W$ is sampled from a density $b(\varphi, \cdot)$ on $W$;

(b) $\varphi' = \varphi \setminus \{\vec{x}\}$, where $\vec{x} \in \varphi$ is chosen with probability $d(\varphi, \vec{x})$ (if $\varphi = \emptyset$ we set $\varphi' = \emptyset$);

(c) $\varphi' = (\varphi \setminus \{\vec{x}\}) \cup \{\vec{y}\}$, where $\vec{x} \in \varphi$ is chosen with probability $d(\varphi, \vec{x})$ and $\vec{y}$ is sampled from a density $m(\varphi \setminus \{\vec{x}\}, \vec{x}, \cdot)$ (if $\varphi = \emptyset$ we set $\varphi' = \emptyset$).

The probability resp. density functions $b$, $d$ and $m$ can be chosen arbitrarily under mild regularity conditions. The proposed state $\varphi'$ is finally accepted with probabilities $\min\{1, r(\varphi, \varphi')\}$, where the Hastings ratio $r(\varphi, \varphi')$ depends on the type of transition and is given by

(a) $$\frac{f(\varphi') p^{\mathrm{del}} d(\varphi', \vec{x})}{f(\varphi) p^{\mathrm{ins}} b(\varphi, \vec{x})};$$

(b) $$\frac{f(\varphi') p^{\mathrm{ins}} b(\varphi', \vec{x})}{f(\varphi) p^{\mathrm{del}} d(\varphi, \vec{x})};$$

(c) $$\frac{f(\varphi') d(\varphi', \vec{y}) m(\varphi \setminus \{\vec{x}\}, \vec{y}, \vec{x})}{f(\varphi) d(\varphi, \vec{x}) m(\varphi \setminus \{\vec{x}\}, \vec{x}, \vec{y})}.$$

If $\varphi'$ is rejected, the Markov chain remains in $\varphi$. If $\varphi = \emptyset$ in case (b) then $r(\varphi, \varphi') = r(\emptyset, \emptyset) = 1$.

In the hard-disk simulations below, $p^{\mathrm{ins}} = p^{\mathrm{del}} = p$ with $0 \le p \le 1/2$, the densities $d(\varphi, \cdot)$ and $b(\varphi, \cdot)$ correspond to the uniform distribution on $W$, and the density $m(\varphi \setminus \{\vec{x}\}, \vec{x}, \cdot)$ is uniform on a square of side length $2 \times \epsilon$ centered in $\vec{x}$. Note that the classical Metropolis algorithm[4] is the special case $p = 0$, i.e., the number of disks is fixed and only moves of disks (case (c)) are allowed.

For large values of $z$ this Markov chain converges very slowly and produces highly autocorrelated samples. As an example we applied the Metropolis-Hastings algorithm with $p = 0.1$ and $\epsilon = 0.3$ for simulation of the process with $W = [0, 10]^2$, $d = 1$, and $\log z = 12.62$. Figure 1 shows time series and estimated autocorrelations for two statistics, viz. the number of points and the empirical mean of the first coordinate of the points in the point pattern. The time series of length 10000 were obtained by subsampling each 5000th state of a chain resulting from $5 \times 10^7$ basic updates (insertions, deletions or moves). Thus, time is measured in units of 5000 basic updates or Monte Carlo sweeps. The time series are highly autocorrelated and the algorithm has not even converged. In particular, the chain stuck after about the first 7000 subsamples. The estimated acceptance probabilities for insertions, deletions and moves are $2 \times 10^{-5}$, $3 \times 10^{-6}$ and 0.12, respectively. (The two first acceptance probabilities have to be equal for a chain in equilibrium.)

### B. Simulated Tempering Algorithm

Much better results are obtained when the Metropolis-Hastings algorithm is combined with simulated tempering as described in the following.

In the case of simulation of hard-disk systems, the equilibrium distribution of simulated tempering is a mixture of repulsive point process models with densities $f_1, \ldots, f_n$, $n \ge 2$, where the Metropolis-Hastings algorithm for $f_i$ mixes well when $i$ is small, while it produces highly autocorrelated samples when $i$ increases towards $n$. Specifically, $f_i$ is chosen as

$$f_i(\varphi) = \frac{1}{\Xi_i} z_i^{\#\varphi} \exp\left( - \sum_{1 \le i < j \le \#\varphi} V_i\left(\|\vec{x}_i - \vec{x}_j\|\right) \right) \tag{3.5}$$

with grand partition functions $\Xi_i$ and pair potential

$$V_i(r) = \gamma_i \left(1 + c\frac{|\mathcal{B}(o, d/2) \cap \mathcal{B}(\vec{r}, d/2)|}{|\mathcal{B}(o, d/2)|}\right) \quad \text{if } r < d, \quad V_i(r) = 0 \quad \text{else,} \tag{3.6}$$

where $\mathcal{B}(\vec{x}, d/2)$ denotes the disk with centre $\vec{x}$ and radius $d/2$ and $|\cdot|$ means area. Both (3.1) and (3.5) are Gibbs process densities, but with different $z$ and different pair potentials. The terms $\gamma_i$ and $\gamma_i c|\mathcal{B}(o, d/2) \cap \mathcal{B}(\vec{r}, d/2)|/|\mathcal{B}(o, d/2)|$ in the pair potential both introduce a penalty whenever two hard disks overlap; the latter term enables to distinguish between point patterns with the same number of overlapping pairs of disks, but with different degrees of overlap. Parameter $c$ describes the balance between these penalties. For the simulations reported in this paper, the value $c = 10$ was chosen as a result of some pilot simulations. If $0 = \gamma_1 < \gamma_2 < \cdots < \gamma_{n-1} < \gamma_n = \infty$ are chosen, then $f_n$ is the hard-core process density (3.1) with $z = z_n$, while $f_1$ specifies the Poisson point process with rate $z_1$. The penalizing parameter $\gamma_i$ can be interpreted as an inverse temperature, so that the Poisson process is the 'hot' distribution and the target process is the "cold" distribution.

Simulated tempering can be described in terms of a Metropolis-Hastings Markov chain $\{(\Phi_l, I_l)\}_{l=0,1,\ldots}$, where $I_l \in \{1, \ldots, n\}$ is a so-called auxiliary variable such that the equilibrium density becomes

$$\tilde{f}(\varphi, i) \propto f_i(\varphi)\Xi_i\delta_i, \quad i = 1, \ldots n, \tag{3.7}$$

where $\delta_i > 0$, $i = 1, \ldots, n$ are user-specified parameters. If $(\Phi, I) \sim \tilde{f}$, then $f_i$ is the conditional density of $\Phi|I = i$ and $P(I = i) \propto \Xi_i\delta_i$.

Good mixing properties of $\{(\Phi_l, I_l)\}$ require that the sojourn probabilities $P(I = i)$ of $I$ are in the same order of magnitude for $i = 1, \ldots, n$. This can be obtained by choosing $\delta_i = 1/(n\hat{\Xi}_i)$, where $\hat{\Xi}_i$ are estimates of $\Xi_i$ which can be obtained in different ways as described in[21]. With this choice of $\delta_i$ an approximate uniform mixture is obtained, i.e., $P(I = i) \approx 1/n$.

Now, for the simulated tempering algorithm transition probabilities $Q(i, j)$ for the auxiliary variables $I_l$ are defined by $Q(i, i + 1) = Q(i, i - 1) = 1/2$ for $1 < i < n$ and

$Q(1,2) = Q(n,n-1) = 1$. Given a current state $(\varphi, i)$, the two components are updated in turn using first the Metropolis-Hastings update $\varphi \to \varphi'$ for the density $f_i(\cdot)$ as in Section A (here $\varphi' = \varphi$ in case the proposal is rejected). Secondly $Q(i,i')$ is used to propose an update $i \to i'$: return $(\varphi', i')$ with probability $\min\{1, r(i,i'|\varphi')\}$ and retain $(\varphi', i)$ otherwise, where

$$r(i,i'|\varphi') = \frac{\tilde{f}(\varphi', i')Q(i',i)}{\tilde{f}(\varphi', i)Q(i,i')} \quad . \tag{3.8}$$

By construction, the Markov chain $\{(\Phi_l, I_l)\}$ is reversible with invariant equilibrium density $\tilde{f}$; in particular, the disk configurations $\Phi_l$ with $I_l = n$ have equilibrium density $f_n$ for $l \to \infty$. It can be shown that the simulated tempering Markov chain has the properties of geometric or uniform ergodicity under mild conditions[32].

Provided that the pairs of parameter values $(z_i, \gamma_i)$ and $(z_{i+1}, \gamma_{i+1})$ are chosen sufficiently close so that reasonable acceptance rates between 20% and 40% for transitions $(\varphi, i) \leftrightarrow (\varphi, i \pm 1)$ are obtained, the disk configurations $\Phi_l$ with $I_l = n$ yield well-mixed samples from the target model $f_n$. Let $(p_i, \epsilon_i)$ denote the parameter values for each of the Metropolis-Hastings algorithms combined in the simulated tempering algorithm, $i = 1, \ldots, n$. The parameter $\epsilon_i$ should be chosen to be decreasing as a function of $i$ so that reasonable acceptance rates for proposed moves are obtained for each temperature. The values of $p_i$ should also be taken to be decreasing since insert or delete proposals have low acceptances probabilities for the low temperatures. The intensity of the initial Poisson point process is chosen as $z_1 = 1/d^2$. This value was chosen because a hard core process with the same mean number of disks as the initial Poisson point process has area fraction $\eta(z) = \pi/4 = 0.785$, nearly the same magnitude as the values of $\eta$ we are interested in our investigations $(0.65 \ldots 0.75)$.

The remaining parameters are chosen as

$$\log z_i = \log z_1 + t_i \left(\log z_n - \log z_1\right) \tag{3.9}$$

and

$$\gamma_i = t_i \gamma^* \quad \text{for } 1 \le i < n, \quad \gamma_n = \infty, \tag{3.10}$$

with $n$ normalized 'temperatures' $0 = t_1 < t_2 < \ldots < t_n = 1$ and a value of $\gamma^*$ such that there are almost no overlapping disks in the $(n-1)$th chain $\{\Phi_l\}_{l \geq 1: I_l = n-1}$. Finally, the adjustment of $n$ and $(t_i)_{i=1,\ldots,n}$ to obtain reasonable acceptance rates for transitions $(\varphi, i) \leftrightarrow (\varphi, i \pm 1)$ is done similarly to[21], Section 2.3. According to these recommendations $n$ took values between 20 and 50 in our simulations.

In Figure 1 the improved time series and estimated autocorrelations are shown for the number of points and the empirical mean of the first coordinate of the points. The relaxation is much faster with simulated tempering than with the usual Metropolis-Hastings algorithm.

## IV. RESULTS FOR HARD DISKS

The following reports on simulation results for the packing fraction and the pair correlation function for the hard-disk system.

For each considered value of $z$ the simulated tempering algorithm was used for the grand canonical ensemble (i.e. all $p_i > 0$) in the simulation study of the packing fraction, while for the pair correlation function the less computer intensive method of simulated tempering for the canonical ensemble (i.e. all $p_i = 0$) was used.

### A. Packing Fraction

Using the periodic boundary condition, the intensity is estimated by $\hat{\lambda}(z) = \overline{N}(z)/|W|$, where $\overline{N}(z)$ is the mean number of disks in the coldest part of the simulated tempering Markov chain. Then the corresponding estimator for the packing fraction $\eta$ is

$$\hat{\eta}(z) = \frac{\pi d^2 \overline{N}(z)}{4|W|}. \tag{4.1}$$

Simulation runs were done for $W = [0, 10]^2$, diameter $d = 1$ and $\log z_n$ between 3 and 14. In the simulated tempering chain, for each considered value of $z$ a sample of length between $5 \times 10^8$ and $10^{10}$ was generated. The calculation of $\overline{N}(z)$ is based on the sample for the cold

chain of length between $2 \times 10^7$ and $10^8$; here an appropriate burn-in (about 10% of the sample) was used. Figure 2 shows the obtained curve of estimated packing fraction $\hat{\eta}(z)$.

In order to test the accuracy of the simulations we use the Padé approximation from Hoover and Ree (1969) for the free energy

$$\frac{\beta F}{N} = \log\left(\lambda\Lambda^2\right) - 1 + b\lambda\frac{1 - 0.28b\lambda + 0.006b^2\lambda^2}{1 - 0.67b\lambda + 0.09b^2\lambda^2} \tag{4.2}$$

where $\Lambda$ is the mean thermal de Broglie wavelength and $b = \frac{\pi}{2}d^2$ yielding

$$\log\frac{z}{\lambda} = \lambda\frac{\partial\beta F/N}{\partial\lambda} + \frac{\beta F}{N} - \log\lambda = \frac{4\eta - 6.04\eta^2 + 3.1936\eta^3 - 0.59616\eta^4 + 0.03456\eta^5}{(1 - 1.34\eta + 0.36\eta^2)^2}. \tag{4.3}$$

The packing fraction $\eta(z)$ above the freezing transition, i.e., for large values of $z$, can be calculated by the free volume theory of Eyring, Kirkwood, and Wood[33–35]. The whole system volume is divided up into similar hexagonal Wigner-Seitz or Dirichlet cells, and the center of each disk is restricted to stay within its own cell. Thus, all configurations are restricted to a solid like structure at high density.

Cell approximations differ in their assumptions about possible shapes of the cell and in the account of multivacancies, i.e., of empty neighboured cells. For the approximation introduced by Wood[35] one obtains $\beta F/N = \log(\lambda\Lambda^2) - 1 - 2\log(1 - \sqrt{\eta/\eta_{cp}})$ and the pressure $\beta P = \lambda/(1 - \sqrt{\eta/\eta_{cp}})$ with the area fraction $\eta_{cp}$ at close packing. Unfortunately, this simple expression does not give the correct absolute free energy of the hard-disk system at very high compressions, i.e., in the limit $\eta \to \eta_{cp}$. Salsburg and Stillinger described a procedure for calculating the asymptotic thermodynamic properties, in particular, the partition function of rigid disk systems in the close packed limit[36,37]. In terms of reduced area $\eta/\eta_{cp}$, where $\eta_{cp} = \frac{\pi}{2\sqrt{3}} \approx 0.907$ is the close-packed value of the covered area fraction in closed system, they find for the free energy

$$\frac{\beta F}{N} \to 2\log\frac{\Lambda}{d} - 2\log(\frac{\eta_{cp}}{\eta} - 1) + C + D(\frac{\eta_{cp}}{\eta} - 1) + \ldots, \tag{4.4}$$

for $\eta \to \eta_{cp}$, with appropriate numerical constants $C$ and $D$. The limiting free energy expression (4.4) may be considered as a 'high density analog of the imperfect gas virial expansion'. The constant $C \approx 0.14370$ can be expressed as an infinite series whose value is

only slightly smaller than the 'single-particle free area' result given by the first summand $C_1 = -\log\sqrt{3/4} \approx 0.14384$. Thus, a single cell of hexagonal shape seems to be a good approximation in order to evaluate $\beta F(\eta)/N$ for values $\eta > \eta_s$ in the solid phase. Assuming that the six nearest neighbours of a disk are located at the corners of a hexagon of edge length $d\sqrt{\eta_{cp}/\eta}$ and area $V = 3/\lambda$ given by the mean density $\lambda$, one can calculate the free area $V_f$ which is accessible for a disk enclosed by its neighbours. Taking into account Kirkwood's communal entropy $\sigma \approx 1$ for the solid phase[34] near close packed configurations, one obtains[36]

$$\beta F/N = \log(\lambda\Lambda^2/\sigma) - \log\left(3\frac{V_f}{V}\right) \tag{4.5}$$

and

$$\frac{V_f}{V} = 1 + \frac{4\eta}{\sqrt{3}\eta_{cp}}\left(\frac{\pi}{6} - \sin^{-1}\sqrt{\frac{\eta_{cp}}{4\eta}}\right) - \sqrt{\frac{4\eta}{3\eta_{cp}} - \frac{1}{3}} \tag{4.6}$$

The factor 3 in the logarithm takes into account that each point of the free volume belongs to three hexagonal cells. Notice that (4.6) exhibits the correct asymptotic limit (4.4) with $C = C_1$. Using thermodynamic relations one immediately obtains the pressure

$$\frac{\beta P}{\lambda} = \lambda\frac{\partial\beta F/N}{\partial\lambda} = \frac{V}{V_f}\left(1 - \sqrt{\frac{4\eta}{3\eta_{cp}} - \frac{1}{3}}\right) \tag{4.7}$$

and the chemical potential

$$\log z = \log(\lambda\Lambda^2) - \log\left(3\frac{V_f}{V}\right) + \frac{\beta P}{\lambda}\,. \tag{4.8}$$

Figure 2 shows that for a wide range of $z$ values the simulated values of $\eta(z)$ nearly coincide with the curves obtained by Padé approximation and the cell model approximation. This indicates that for values of $\log z < 9$ (corresponding to $\eta < 0.65$) both the Padé formula and the simulations yield similar approximations of $\eta(z)$ which can be assumed to be close to the true values. For values of $\log z > 13.5$ the cell model approximation yields values of $\eta(z)$, which are in good agreement with the simulated tempering simulation results. This may indicate that this approximation is of good quality for the larger $z$. Obviously, the $\hat{\eta}(z)$

curve shows an irregularity around $\log z = 13.3$. The question is whether there is a jump of $\eta(z)$, in other words a phase transition of first order. The values obtained by our simulations may indicate that there is a jump but the data are not conclusive. The cell approximation shows that the two states joined by a tie line in the simulation data do have the same chemical potential, and are therefore in thermodynamic equilibrium.

The chemical potential $\log z$ is larger in the simulation than the tie line potential which would have been expected for a first order transition between $\eta_f = 0.69$ and $\eta_s \approx 0.72$. It could be conjectured that the simulations were probing metastable states on the fluid branch of the van der Waals loop until fluid structure becomes unstable at $\log z \approx 13.3$.

### B. Pair Correlation Function

For determining the pair correlation function $g(r)$ canonical ensembles of disks with diameter $d = 1$ on a square of edge length 20 were simulated. The fixed number $N$ of disks for every value of packing fraction $\eta = 0.65$, 0.67, 0.69, 0.696, 0.701, 0.707, 0.71, 0.715, 0.721, 0.735 was chosen so that $\eta = \pi d^2 N/(4|W|)$. Hence $N$ is ranging from 331 to 374. The pair correlation function was then estimated from 100 independent disk patterns of the cold chain obtained from much longer runs of the simulated tempering chain. Because of the small changes in the simulated tempering chain, estimates based on subsequent point patterns look almost the same. Therefore, for the 100 point patterns a spacing of at least $10Nn$ was used.

Figure 3 shows estimated pair correlation functions for $\eta = 0.65$ and $\eta = 0.735$ which are in very good agreement with the results in Truskett *et al.*[25] obtained by molecular dynamics.

As expected, for the larger $\eta$ the pair correlation function reflects more order. The peaks of the estimated pair correlation functions can be compared with the modes at $r = 1, \sqrt{3}, 2, \ldots$ for the pair correlation function of the limiting regular hexagonal pattern of hard disks with diameter $d = 1$. Clearly the curve for $\eta = 0.735$ is in better agreement to the limiting case than the curve for $\eta = 0.65$. In particular, the second mode for the curve with $\eta = 0.65$

splits into two modes as $\eta$ increases.

### C. Alignment function

The alignment function $z_B(r)$ is a kind of third-order characteristic which is well adapted to show if there are linear chains of points as for lattice-like point patterns (Stoyan and Stoyan[38]). For $r > 0$, consider any vector $\vec{r}$ with $\|\vec{r}\| = r$ and let $B_r$ be a square centered at $\vec{r}/2$ and of side length $\alpha r$, where one side is parallel to $\vec{r}$ and $0 < \alpha < 1$ is a user-specified parameter (in Figure 4, $\alpha = 0.1$). We can interpret $\lambda|B_r|z_B(r)$ as the mean number of points in $B_r$ under the condition that there is a point in the origin $o$ and another point located at $\vec{r}$. Large and small values of $z_B(r)$ for suitable $r$ indicate a tendency of alignment in the point pattern:

- For a stationary Poisson point process, $z_B \equiv 1$.
- If $z_B(r) > 1$ then $B_r$ contains in the average more points than an arbitrarily placed rectangle of the same area. An example for this case is distance $r = 2$ in a regular hexagonal pattern of disks with diameter 1. If $\alpha$ is sufficiently small there is always one disk centre inside $B_2$, moreover, this centre coincides with the centre of $B_2$. Therefore, $z_B(2) = 1/(\lambda|B_2|) = 1/(2\sqrt{3}\alpha^2)$, which tends to infinity for $\alpha \to 0$.

Owing to these considerations, one may expect $z_B(2)$ to be an increasing function of $\eta$ with limit $0.2165/\alpha^2$ obtained at the maximum area fraction $\eta_{cp} = \frac{\pi}{2\sqrt{3}} \approx 0.907$.

The statistical estimation of $z_B(r)$ follows[38], page 294, except that we again replace $\lambda$ with $N/|W|$ (since the number of points is fixed) and use the torus convention.

Our simulations show as expected that $z_B(2)$ increases with increasing $\eta$; but $z_B(2) = 1.83$ for $\eta = 0.735$ and this is still far from the maximum value 21.65 at $\eta = 0.907$. The alignment of the point patterns is more apparent for slightly increased $r$, e.g. $r = 2.2$. Figure 4b shows estimates of $z_B(2.2)$ and $z_B(3)$ as functions of $\eta$. Also $z_B(2.2)$ is an increasing function of $\eta$. Note that the curve of $z_B(2.2)$ is steepest for values of $\eta$ between the freezing ($\eta_f = 0.69$)

and melting ($\eta_s = 0.73$) points. The value 14.96 of $z_B(2.2)$ for $\eta = 0.735$ is not very far from the upper bound 17.89 obtained by assuming that $\lambda|B_{2.2}|z_B(2.2) \leq 1$.

### D. Hexagonality number

The idea behind any hexagonality characteristic is to look for deviations from the hexagonal arrangement of neighbouring points to a point in an equilateral triangular lattice.

A first possibility is to use Ripley's $K$ function (see e.g.[38]). Here $\lambda(z)K(r)$ is the mean number of points in a disk of radius $r$ centered at a typical point (which is not counted). In the case of an equilateral triangular lattice with side length 2, $K(r)$ vanishes for $r < 1$ and takes the value 6 for values of $r$ a bit larger than 1. Thus, for the hard core Gibbs point process when $r$ is a bit larger than 1 and the number of points is fixed, one should expect an abrupt change of the values of $K(r)$ for $\eta$ in the phase transition region. This, however, was not observed in our simulations, where we observed a continuous and nearly linear dependence of $K(1.3)$ on $\eta$.

Quite different is the behaviour of the 'hexagonality number' $H(r)$, the *probability* that a disk of radius $r$ centered at the typical point contains exactly 6 other points. Figure 4c shows the estimated $H(1.3)$ as an increasing function of $\eta$. The curve is steepest when $\eta$ is between the freezing and melting points.

Weber *et al.* (1995) consider another characteristic, the bond orientational number $\psi(r)$ defined as the norm of the mean of the following sum taken over all points of the hard core Gibbs point process contained in a disk of radius $r$ centered at the $k$-th point: $\sum_j e^{6i\phi_{kj}}$, where $i$ denotes the imaginary unit and $\phi_{kj}$ is the angle between the $x$-axis and the line through point $k$ and its $j$th neighbor point in the disk. An estimate of $\psi(r)$ is given by

$$\hat{\psi}(r) = \left| \frac{1}{N_{\text{bond}}} \sum_k \sum_j e^{6i\phi_{kj}} \right| \tag{4.9}$$

where $k$ runs over all points in the system, $j$ runs over all neighbors of $k$ and $N_{\text{bond}}$ denotes the number of bonds $(k, j)$. Clearly, this characteristic quantifies very well the degree of

hexagonality in a point pattern. The estimated $\psi(1.3)$ shown in Figure 4c as function of the packing fraction $\eta$ is similar to $H(1.3)$.

The bond orientational $\psi$ and the hexagonality number $H$ are expected to vanish for $\eta < \eta_f$ and to have finite values less than unity for $\eta > \eta_s$. For the transition regime $\eta_f < \eta < \eta_s$ both quantities should increase linearly in case of an first order transition according to the lever rule but should vanish throughout a hexatic phase and jump at $\eta_s$ in case of the Kosterlitz-Thouless scenario. Thus, ignoring finite size effects, one could determine the nature of the transition just by measuring $\psi(r)$ or $H(r)$. Although the finite size of the system could change the functional shape qualitatively, the linear increase clearly visible in Fig. 4c indicates a first order melting transition.

## V. CONCLUSIONS

The melting transition of hard disks in two dimensions is still an unsolved problem and improved simulation algorithms are needed for its investigation. We presented the simulated tempering method for grand canonical ensembles as an efficient alternative to commonly used Metropolis-Hastings algorithms for canonical and grand canonical hard-disk systems. This approach allows the direct study of thermodynamic quantities such as pressure and packing fraction as function of the chemical potential. Fluctuating particles numbers yield configurational changes even at large scales and at high densities which finally decrease the persistence of a metastable solid phase. Moreover, grand canonical simulations are capable to determine directly the entropy in the solid phase and to overcome constraints on lattice configurations induced by periodic boundary conditions. We considered the two-dimensional hard-disk system in order to compare the techniques in detail. The packing fraction $\eta(z)$ for values of the fugacivity $z$ below the freezing point is in very good agreement with Padé approximations. Moreover, the simulated tempering simulations yield good agreement with analytical results even close above the melting point. The simulations indicate a first order phase transition, but the results differ from those of other simulations and have to be con-

firmed. Further applications of the simulated tempering technique might help to resolve the order and type of the phase transition in hard-disk systems.

## ACKNOWLEDGMENTS

JM and RW were supported by the European Union's network 'Statistical and Computational Methods for the Analysis of Spatial Data. ERB-FMRX-CT96-0095', by MaPhySto – Centre for Mathematical Physics and Stochastics, funded by a grant from the Danish National Research Foundation – and by the Danish Informatics Network in the Agricultural Sciences, funded by a grant from the Danish Research Councils. DS was supported by a grant of Deutsche Forschungsgemeinschaft. We are grateful to Salvatore Torquato for helpful comments.

# REFERENCES


[1] B. J. Alder and T. E. Wainwright, *Phys. Rev.* **127**, 359 (1962).

[2] D. R. Nelson and B. I. Halperin, *Phys. Rev. B* **19**, 2457 (1979); A. P. Young, *Phys. Rev. B* **19**, 1855 (1979).

[3] J. M. Kosterlitz and D. J. Thouless, *J. Phys. C* **6**, 1181 (1973); J. M. Kosterlitz, *J. Phys. C* **7**, 1046 (1974); V. L. Berenzinskii, *Sov. Phys. JETP* **34**, 610 (1972).

[4] N. Metropolis, A. W. Rosenbluth , M. N. Rosenbluth, A. H. Teller and E. Teller, *J. Chemical Physics* **21**, 1087–1092 (1953).

[5] M. P. Allen and D. J. Tildesley, *Computer Simulation of Liquids*. Oxford University Press, Oxford (1987).

[6] K. J. Strandburg, *Rev. Mod. Phys.* **60**, 161–207 (1988).

[7] K. Binder (Ed.), *Topics in Applied Physics* Vol. 71, Springer, Berlin (1995).

[8] G. Ciccotti, D. Frenkel, I. R. McDonald (Eds), *Simulation of liquids and solids. Molecular Dynamics and Monte Carlo Methods in Statistical Mechanics*, North-Holland, Amsterdam (1987).

[9] D. Frenkel and B. Smit, *Understanding molecular simulation. From algorithms to applications*. Academic Press, San Diego (1996).

[10] J. A. Zollweg, G. V. Chester, and P. W. Leung, *Phys. Rev. B* **46**, 11186 (1992).

[11] H. Weber and D. Marx, *Europhys. Lett.* **27**, 593 (1994).

[12] H. Weber, D. Marx, and K. Binder, *Phys. Rev. B* **51**, 14636 (1995).

[13] J. Lee and K. J. Strandburg, *Phys. Rev. B* **46**, 11190 (1992).

[14] J. Fernandez, J. J. Alonso, and J. Stankiewicz, *Phys. Rev. Lett.* **75**, 3477 (1995).

[15] W. G. Hoover and F. H. Ree, *J. Chem. Phys.* **49**, 3609 (1969).

[16] M. Schmidt, *Freezing in confined geometry*, PhD-thesis Düsseldorf 1997; Shaker Verlag, Aachen (1997).

[17] K. Bagchi, H. C. Andersen, and W. Swope, *Phys. Rev. Lett.* **76**, 255 (1996).

[18] A. H. Marcus and S. A. Rice, *Phys. Rev. Lett.* **77**, 2577 (1996).

[19] A. Jaster, *cond-mat/9810274* (21. Oct. 1998); *Physica A* **264**, 134 (1999).

[20] W. C. Swope and H. C. Andersen, *Phys. Rev. A* **46**, 4539 (1992); *J. Chem. Phys.* **102**, 2851 (1995).

[21] C. J. Geyer and E. A. Thompson, *J. Am. Statist. Ass.* **90**, 909–920 (1995).

[22] E. Marinari and G. Parisi, *Europhysics Letters* **19**, 451–458 (1992).

[23] J.-P. Hansen and I. R. McDonald, *Theory of Simple Liquids*. Academic Press, London (1986).

[24] W. G. Hoover and F. H. Ree, *J. Chem. Phys.* **49**, 3609–3617 (1969).

[25] T. M. Truskett, S. Torquato, S. Sastry, P. G. Debenetti and F. H. Stillinger, *Phys. Rev.* E **58**, 3083–3088 (1998).

[26] A. C. Mitus, H. Weber and D. Marx, *Phys. Rev.* E **55**, 6855–6859 (1997).

[27] H. Weber, D. Marx and K. Binder, *Phys. Rev.* B **51**, 14636–14651 (1995).

[28] C. J. Geyer and J. Møller, *Scand. J. Statist.* **21**, 359–373 (1994).

[29] C. J. Geyer, *Stochastic Geometry: Likelihood and Computations* (eds. O. E. Barndorff-Nielsen, W. S. Kendall and M. N. M. van Lieshout), pages 79–140. Chapman and Hall/CRC, London (1999).

[30] J. Møller, *Stochastic Geometry: Likelihood and Computations* (eds. O. E. Barndorff-Nielsen, W. S. Kendall and M. N. M. van Lieshout), pages 141–172. Chapman and Hall/CRC, London (1999).

[31] C. J. Geyer, *Technical report No. 568*, School of Statistics, University of Minnesota (1993).

[32] S. Mase, J. Møller, D. Stoyan, R. P. Waagepetersen and G. Döge, Packing Densities and Simulated Tempering for Hard Core Gibbs Point Processes. *Research report No. 12*, Department of Mathematical Sciences, Aalborg University (1999).

[33] H. J. Eyring and O. Hirschfelder, *J. Chem. Phys.* **41**, 250 (1937); Lennard-Jones and Devonshire, *Proc. Roy. Soc. A* **163**, 53 (1937); **165**, 1 (1938).

[34] J. G. Kirkwood, *J. Chem. Phys.* **18**, 380 (1950).

[35] W. W. Wood, *J. Chem. Phys.* **20**, 1334 (1952).

[36] F. H. Stillinger, Z. W. Salsburg and R. L. Kornegay, *J. Chem. Phys.* **43**, 932–943 (1965).

[37] Z. W. Salsburg, W. G. Rudd and F. H. Stillinger, *J. Chem. Phys.* **47**, 4534–4539 (1967).

[38] D. Stoyan and H. Stoyan, *Fractals, Random Shapes and Point Fields.* Wiley & Sons, Chichester (1994).

# FIGURE CAPTIONS

**FIGURE 1.**

Time series and estimated autocorrelations obtained with the Metropolis-Hastings algorithm (left column) and for the coldest chain in simulated tempering (right column). (a) number $\#\varphi$ of points, (b) autocorrelation function of $\#\varphi$, (c) first coordinates in the point pattern, and (d) autocorrelation function of them. Time is measured in units of 5000 Monte Carlo sweeps. Whereas for the usual Metropolis-Hastings algorithm the configurations are highly autocorrelated and the convergence to equilibrium is very slow, the relaxation is much faster with Simulating Tempering.

**FIGURE 2.**

Estimated values of $\eta(z)$ using simulated tempering (+), Padé approximation (broken line) and cell approximation (dotted line). A first order transition is found between $\eta_f \approx 0.69$ and $\eta_s \approx 0.73$.

**FIGURE 3.**

Estimated pair correlation functions for $\eta = 0.65$ (dashed line) and $\eta = 0.735$ (solid line).

**FIGURE 4.**

Various spatial characteristics of the pure hard core process versus area fraction: (a) Estimated values of the packing fraction $\eta(z)$ using samples obtained with the simulated tempering algorithm. Note that $\eta$ is smaller for $12.7 < \log z < 13.3$ than in an expected solid phase when a first order transition occurs between $\eta_f \approx 0.69$ and $\eta_s \approx 0.73$. Probably the simulations did probe metastable states on the fluid branch of the van der Waals loop until fluid structure becomes unstable at $\log z \approx 13.3$. Therefore, the value $\eta_s \approx 0.73$ for the melting density might be too large. (b) The alignment functions $z_B(r)$ for various distances $r$ normalized by its value at $\eta = 0.65$, namely $z_B(2) = 0.894$, $z_B(2.2) = 6.423$, $z_B(2.5) = 2.589$, $z_B(3) = 0.236$, $z_B(3.2) = 0.155$, $z_B(3.5) = 0.397$, $z_B(4) = 1.481$. (c) Estimated hexagonality number $H(1.3)$ (triangles) and bond orientational number $\psi(1.3)$ (circles).

FIGURE 1

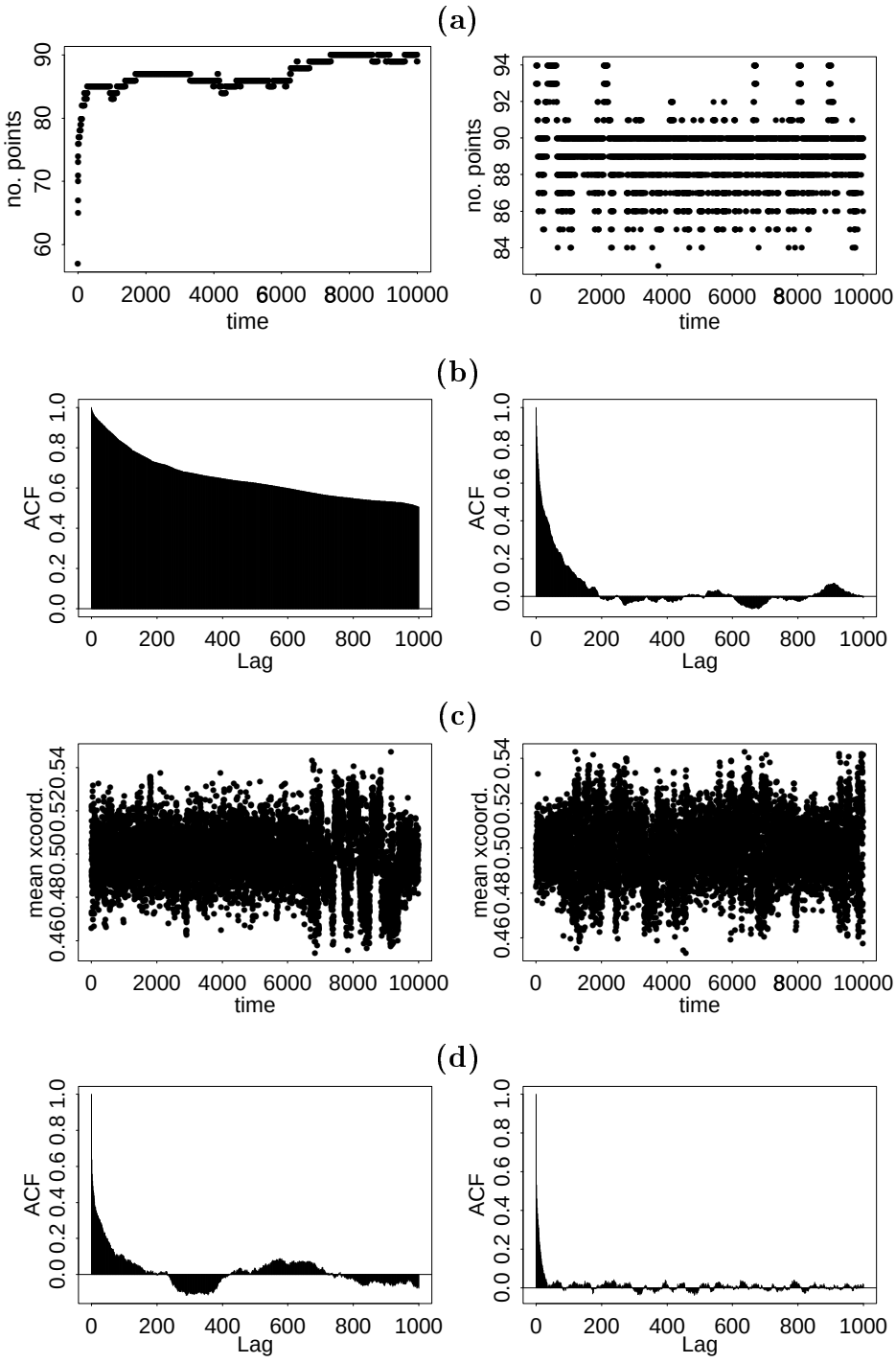

FIGURE 2

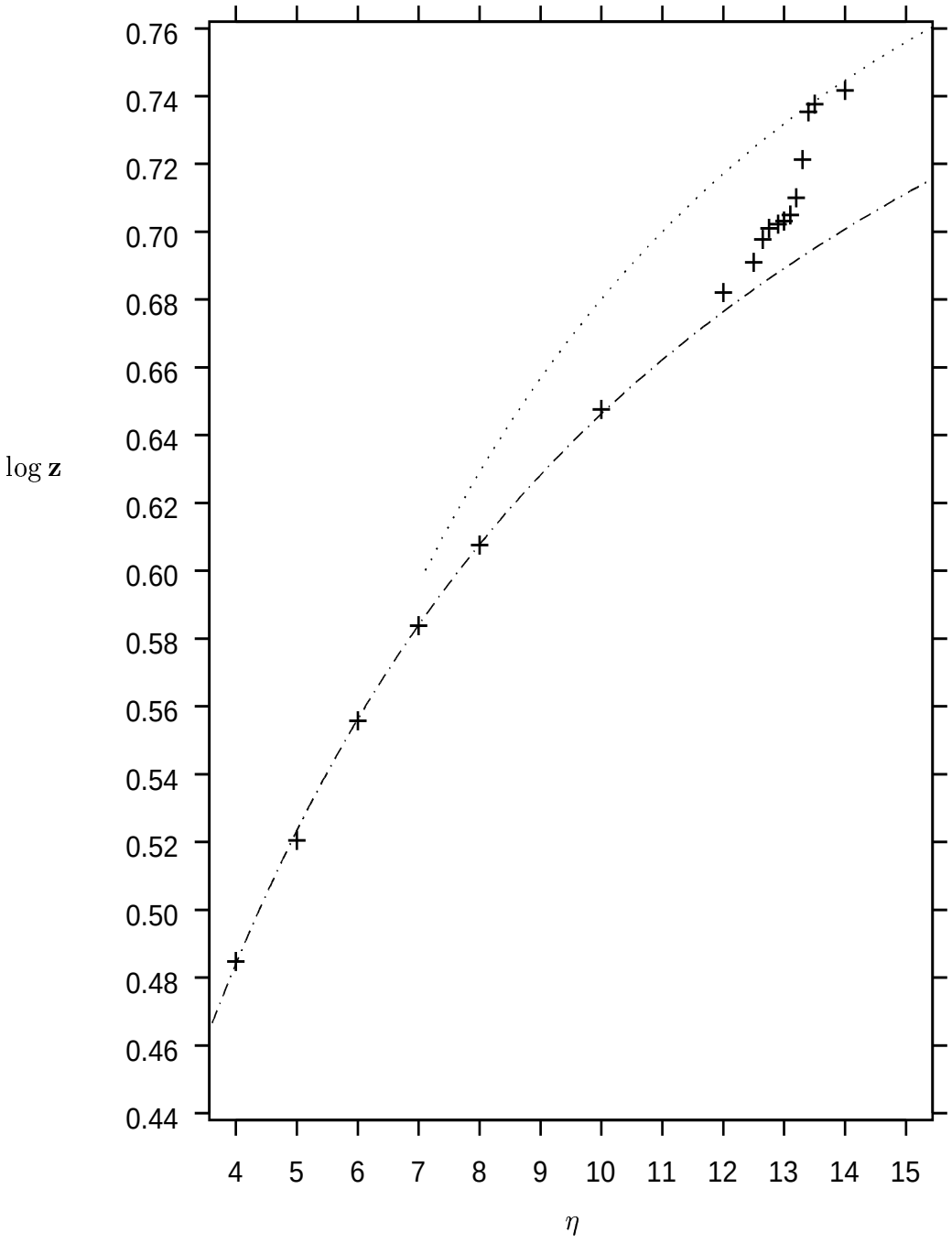
log z
0.76
0.74
0.72
0.70
0.68
0.66
0.64
0.62
0.60
0.58
0.56
0.54
0.52
0.50
0.48
0.46
0.44
4
5
6
7
8
9
10
11
12
13
14
15
η

FIGURE 3

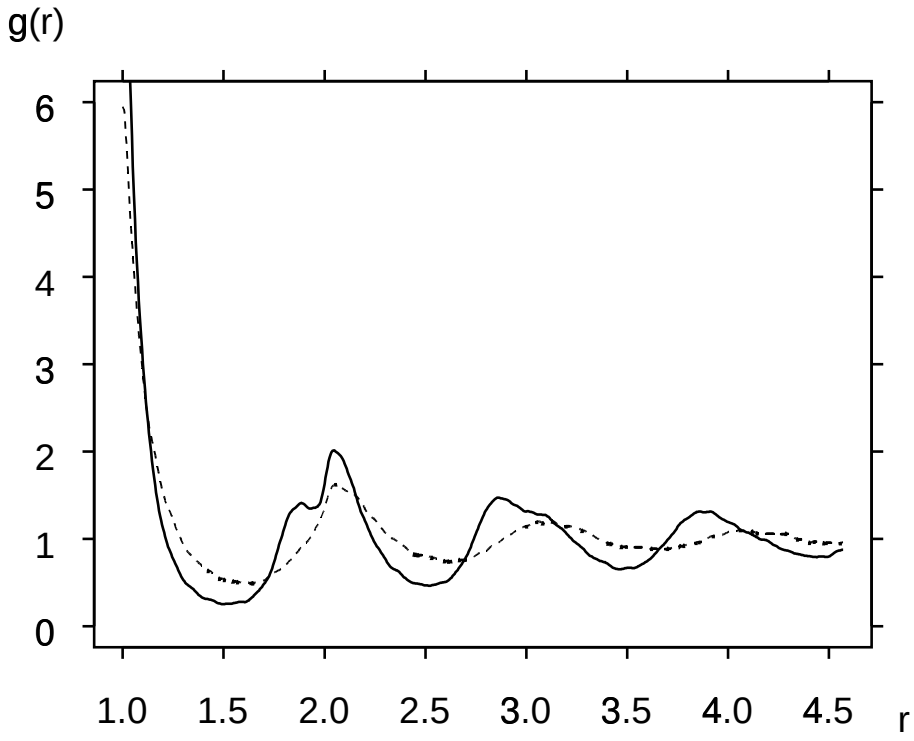

FIGURE 4

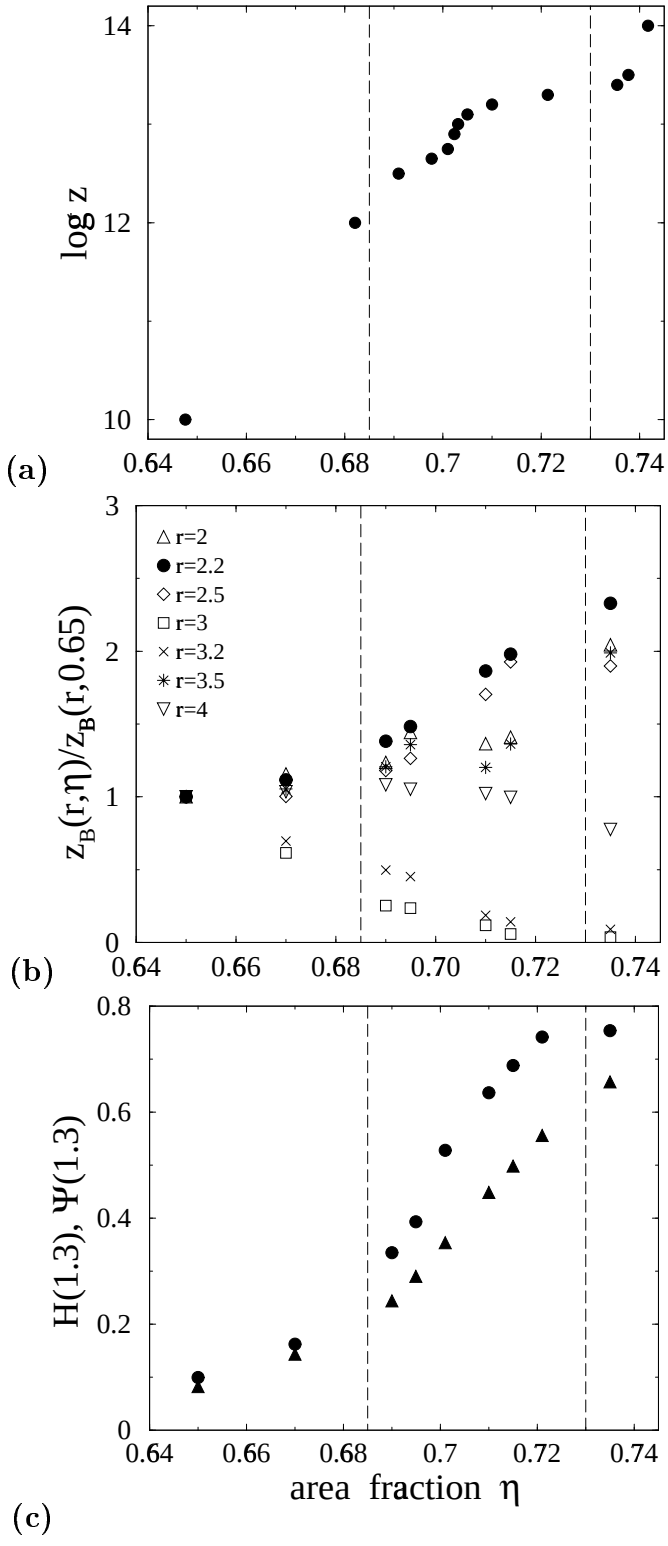
14
12
10
log z
0.64
0.66
0.68
0.7
0.72
0.74
(a)
3
2
1
0
$z_B(r,\eta)/z_B(r,0.65)$
r=2
r=2.2
r=2.5
r=3
r=3.2
r=3.5
r=4
0.64
0.66
0.68
0.70
0.72
0.74
(b)
0.8
0.6
0.4
0.2
0
H(1.3), Ψ(1.3)
0.64
0.66
0.68
0.7
0.72
0.74
area fraction η
(c)